CrossMark

Photocatalytic degradation of methylene blue by hydrothermally synthesized CZTS nanoparticles

Shilpa A. Phaltane[1] · S. A. Vanalakar[2] · T. S. Bhat[2] · P. S. Patil[2] · S. D. Sartale[3] ·
L. D. Kadam[1]

Abstract Due to the toxic effect of Methylene blue (MB) dye, its removal from water and water waste has gained significant attention in concern with green environment. In present work, a simple and low cost hydrothermal method has been used for the synthesis of copper zinc tin sulfide (CZTS) nanoparticles. Structural, morphological and optical properties of CZTS nanoparticles were characterized and it reveals that the synthesized powder has kesterite crystal structure with agglomerated morphology and shows a band gap of 1.53 eV leading to good potential to degrade methylene blue dye. When CZTS was introduced in aqueous MB solution as a catalyst and exposed to visible light for 45 min, about 50% degradation of MB was observed.

1 Introduction

One cannot imagine life without water. A fast development in industrial sector improves human living standard but at the same time it plays major role in earth pollution. This growth increases the demand of water supply. The domestic use and industrial growth produces large amount of water waste, when disposed in nature it results in harmful impact on earth atmosphere. Among different industries, a textile industry uses large amount of water for treatments like dyeing and washing of fabrics. Waste water from these treatments is affected by dyes which cause harmful impact on living organisms. Photocatalysis is a promising method for solving environmental problems, especially for the removal of organic contaminants from textile industrial water disposal. Semiconductor photocatalysis is one of the important techniques for treatment of contaminants as it uses sunlight to decompose organic pollutants [1].

In semiconductor photocatalysis, when material is exposed to light radiation electron hole pair generated. Electrons go to conduction band by creating hole in valence band who react with pollutant via oxidation and reduction process. So, photocatalyst must be photoactive, absorbs maximum solar radiation, chemically stable, non toxic and economical [2]. TiO_2, ZnO, CdS are well known n type of photocatalyst materials but they have wider band gap [3–5]. Less research is going on p-type of photocatalyst.

A low cost solar absorbing material with high absorption coefficient and direct band gap has attracted much more attention. Now-a-days copper zinc tin sulfide Cu_2ZnSnS_4 (CZTS) is a promising material as its constituents are eco-friendly, non-toxic, earth abundant, low cost and its absorption coefficient is also high ($\sim 10^4$ cm^{-1}) [6, 7]. It is a quaternary p-type semiconducting material which possesses potential to be used in energy harvesting, thermoelectric as well as photocatalytic applications [8–11]. CZTS was reported by Katagiri for the first time [12]. After that different methods were used for the synthesis of CZTS such as microwave [13], Sol–Gel [14], solvothermal [15], SILAR [16], Hot injection [17], Electrodeposition [18], Sputtering [19], Pulse laser deposition [20], Hydrothermal [21].

✉ L. D. Kadam
    kdlaxman_222@yahoo.co.in

    Shilpa A. Phaltane
    shilpa.phaltane@gmail.com

1   Solid State Physics Laboratory, Department of Physics, Yashvantrao Chavan Institute of Science, Satara, Maharashtra 415001, India

2   Thin Film Materials Laboratory, Department of Physics, Shivaji University, Kolhapur, Maharashtra 416004, India

3   Thin Films and Nanomaterials Laboratory, Department of Physics, Savitribai Phule Pune University, Pune 411007, India

Among these methods, hydrothermal has been widely used due to the simpler procedure, eco-friendly and economical nature. The research is focused on such multifunctional material that can be used in different applications [8, 22–26]. This boosted our interest for the synthesis of CZTS via hydrothermal route. Herein we report synthesis of kesterite phase CZTS nanoparticles and its use is as a catalyst in photocatalytic degradation of methylene blue dye.

2 Experimental method

All chemicals used for synthesis of CZTS were analytical reagent (AR) grade. For synthesis of CZTS, 0.08 M Copper(I) chloride (CuCl), 0.04 M Zinc(II) chloride (ZnCl$_2$), 0.04 M tin(IV) chloride pentahydrate (SnCl$_4$·5H$_2$O) and 0.32 M thiourea SC(NH$_2$)$_2$ were used as precursors in the molar ratio (2:1:1:8). They were dissolved in 40 ml mixed solvent of ethanol and water (1:1) under magnetic stirring at room temperature, then, obtained solution was transferred into 50 ml Teflon-lined stainless steel autoclave. Sealed autoclave was kept in muffle furnace at 210 °C for 24 h. After natural cooling to room temperature final product was centrifuged and washed with double distilled water several times to remove water soluble impurities and finally dried it overnight at 60 °C. To obtain pure phase and more crystalline nature of CZTS, synthesized powder was annealed in presence of sulfur powder at 500 °C under N$_2$ gas for 30 min in tubular furnace.

2.1 Characterizations of CZTS powder

The XRD patterns were recorded using X-ray powder diffractometer (Bruker AXS Analytical Instruments Pvt. Ltd., Germany, Model: D2 phaser) with Cu Kα radiation. The surface morphology of the CZTS powder was recorded by a scanning electron microscope (SEM; S-4700, Hitachi). Raman spectra were recorded using Renishaw InVia micro-Raman spectrometer using an excitation source of 532 nm laser. The scattered light was analyzed by using charge coupled device (CCD) detector. The room temperature optical absorption measurements were performed in the wavelength range over 100–1000 nm by using a UV–Vis spectrophotometer (UV1800, Shimadzu, Japan).

2.2 Photocatalytic activity measurement

To study photocatalytic activity, 100 ml of aqueous MB solution (initial concentration: 70 mg/lit) was used in the presence of 25 mg of CZTS powder under the visible light radiation. Prior to irradiation, solution was ultra-sonicated for 10 min. and then magnetically stirred in dark for 6-h to achieve adsorption equilibrium. The

concentration of methylene blue was determined by UV–Vis spectrometer. A sample of about 5 ml was taken to determine the initial concentration prior to illumination. The photocatalyst was irradiated from top with a visible light. Continuous stirring was performed using a magnetic stirrer. After every 10 min, 5 ml of solution was pipette out, centrifuged and the absorbance of the clear supernatants was determined at 664 nm wavelength for methylene blue against appropriate blanks. The catalytic degradation efficiency (%) for annealed CZTS powder sample was calculated as:

$$\text{Efficiency of degradation } (\%) = 100\left(\frac{A_o - A_t}{A_o}\right) \quad (1)$$

where A$_o$ = dye solution absorbance in absence of catalyst, A$_t$ = dye solution absorbance in presence of catalyst after time t. According to first order kinetics reaction, rate constant 'k$_{app}$' was determined by using the relation:

$$\ln\left(\frac{A_t}{A_o}\right) = -k_{app}t \quad (2)$$

3 Result and discussion

3.1 Structural analysis (XRD)

The XRD patterns of synthesized and annealed samples are shown in Fig. 1. As-synthesized sample shows three major peaks at 2θ = 28.46°, 47.27° and 55.56° can be attributed to the diffraction from (112), (220) and (312) planes respectively. After annealing intensity of
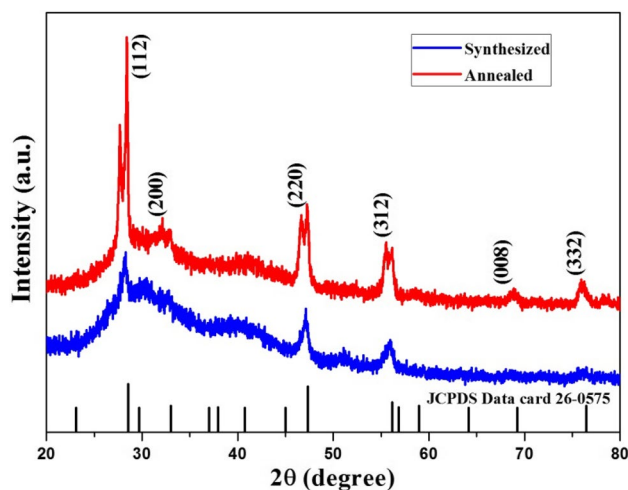

Fig. 1 XRD pattern of synthesized and annealed nanoparticles. The fine line shows the simulated pattern of kesterite CZTS (JCPDS no. 26-0575)

major peaks increases indicating increase in crystalline nature of powder samples [27]. Along with major peaks annealed sample shows minor peaks at 32.11°, 69.05° and 76.10° attributed to the (200), (008) and (332) planes. Diffraction peaks match well with the JCPDS data card 26-0575 reveal that the synthesized power has kesterite CZTS phase [21, 28–31]. The lattice parameters for the tetragonal structure can be calculated by the expression:

$$\frac{1}{d^2} = \frac{h^2 + k^2}{a^2} + \frac{l^2}{c^2} \tag{3}$$

The observed mean values of the lattice parameter (a = 5.57 Å, c = 10.33 Å) are calculated from XRD peaks which match well with the JCPDS card 26-0575 (a = b = 5.43 Å, c = 10.84 Å). The standard and observed 'd_{hkl}' values with their respective planes of the annealed sample were calculated by using Bragg's law: $2d_{hkl}\sin\theta = n\lambda$ are summarized in following Table 1:

Using Scherer's formula,

$$D = \frac{0.9\lambda}{\beta \cos\theta} \tag{4}$$

The crystallite size can be calculated, where β is full width half maxima (FWHM), λ is the X-ray wavelength. The average crystallite size of annealed sample using the (112) plane's reflection is 29 nm. No secondary phases are detected in XRD pattern indicating the phase purity of the product. But for the confirmation of CZTS phase, Raman analysis is performed. Because the secondary phases like ZnS and Cu_2SnS_3 have similar lattice parameters [16]. Hence, synthesized and annealed powders are further characterized by Raman spectroscopy.

3.2 Raman analysis

The room temperature micro Raman spectra of synthesized and annealed samples were carried out with the help of 532 nm laser in the range of 100–600 cm^{-1}, is shown in Fig. 2. As per the literature, most intense peak position in the range 331–338 cm^{-1} and minor peak at 285 cm^{-1}

Table 1 The standard and observed 'd_{hkl}' values with their respective planes of the annealed sample

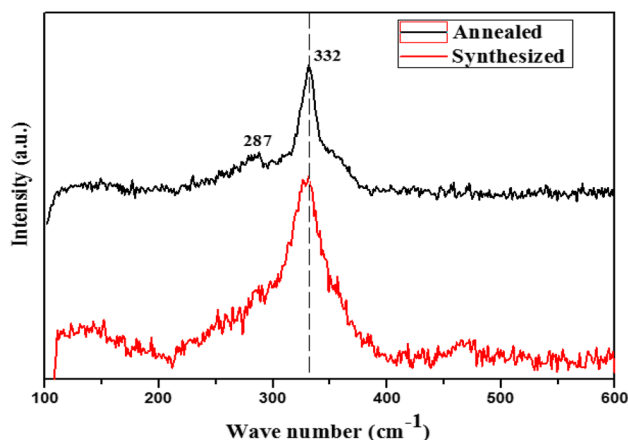| Sr. no.	2θ (in degree)		Plane (hkl)	'd' spacing (in Å)	
	Standard	Observed		Standard	Observed
1	28.53	28.46	(112)	3.1260	3.133
2	32.99	32.11	(200)	2.7130	2.785
3	47.33	47.27	(220)	1.9190	1.921
4	56.17	55.56	(312)	1.6360	1.653
5	69.22	69.05	(008)	1.356	1.359
6	76.43	76.10	(332)	1.2450	1.250

Fig. 2 Raman spectrum of the synthesized and annealed CZTS powder

has been reported. We observed a most intense peak at 332 cm^{-1} and minor peak at 287 cm^{-1} which match well with the reported [21, 32]. Intense peak can be assigned to A1 mode of vibration of sulfur atoms surrounded by motionless neighboring atoms [32]. The broadening of this peak indicates the phonon confinement effect due to smaller size of nanoparticles which is given by Heisenberg's uncertainty principle: $\Delta X . \Delta P \geq \frac{h}{2\pi}$: where ΔX is particle size, ΔP is phonon momentum distribution, h is Planks constant. This shows that reduction in particle size results in confinement of phonon within the particle. FWHM of peak at 332 cm^{-1} was calculated to be 20 cm^{-1}. This line width is strongly governed by the time scale of the de-excitation process can be derived from energy time uncertainty relation:

$$\frac{1}{\tau} = \frac{\Delta E}{\hbar} = 2\pi c \Gamma \tag{5}$$

where ΔE is uncertainty in phonon energy state, h is planks constant, c is velocity of light and Γ is FWHM of highly intense Raman peak in cm and τ is mean phonon life time. Using this relation mean phonon life time (τ) of annealed CZTS sample was calculated to be 0.2653×10^{-12} s [33]. Raman spectra of annealed sample reveal that sharpness of the most intense peak increases on annealing which indicates good crystalline nature [21].

3.3 SEM analysis

Microstructure and surface morphology play very important role for different optoelectronic applications of inorganic semiconducting material. Figure 3 shows SEM images of annealed sample which represent the surface morphology of CZTS powder. It reveals that CZTS powder is agglomeration

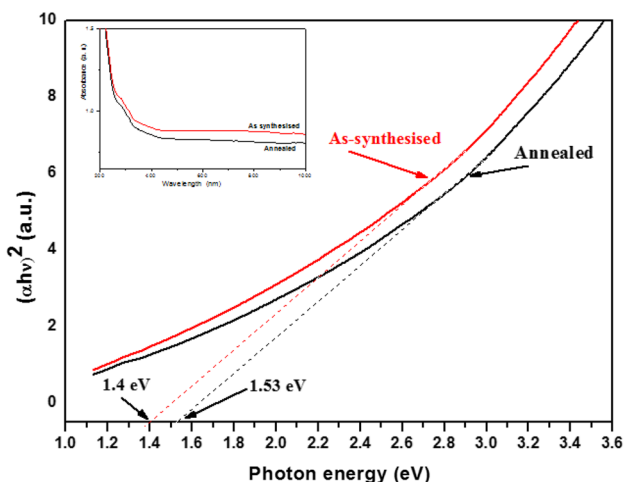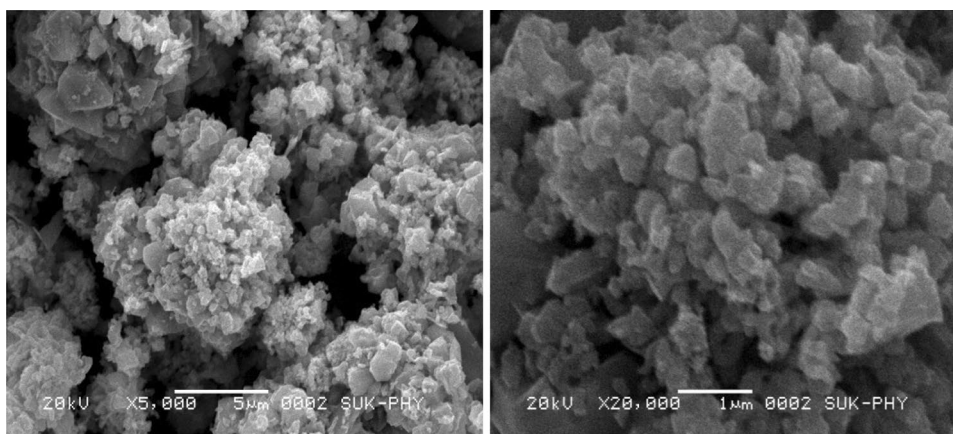**Fig. 3** SEM image CZTS powder annealed at 500 °C

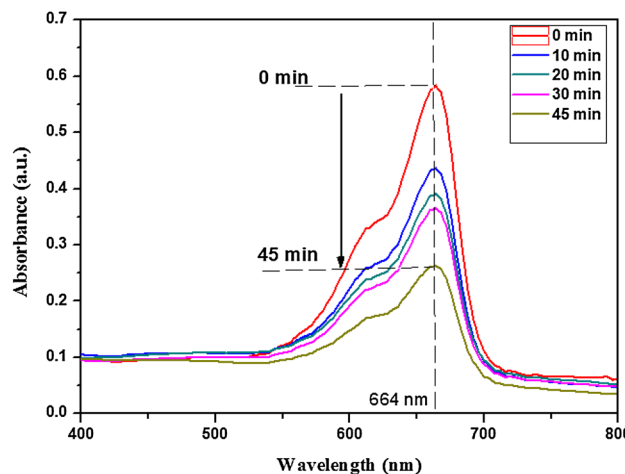**Fig. 4** Tauc plot for measurement of band gap (*inset* UV–Vis absorption spectrum)

Fig. 5 UV–Vis absorption spectra of degradation of 100 ml MB aqueous solution under a visible light radiation in presence of 25 mg of CZTS

of nanoparticles. This agglomeration could be attributed to high surface energy with smaller size [34].

3.4 UV Visible spectroscopy

Optical absorbance measurement was used to determine the band gap of CZTS sample. It was determined by using the liquid phase method. The sample was ultrasonically dispersed in iso- propanol for few minutes and then transferred to cuvette for measurement of absorption. Both the samples exhibit broad absorption in visible region; whereas the tail of graph extends to the longer wavelength. Strong absorption spectra indicate its usefulness in photovoltaic and photocatalytic application. Tauc and Davise Mott model was used to obtain optical band gap by using equation:

$$(\alpha h\gamma)^n = A\left(h\gamma - E_g\right) \tag{6}$$

where A is absorbance, E_g is band gap, $h\gamma$ is the incident photon energy, α is absorption coefficient and n is index characterizing the type of optical transition. The value of n is taken as 2 for direct band gap material. Figure 4 shows the UV–Vis spectra of synthesized and annealed powder samples. By extrapolating the linear part of the graph of $(Ah\gamma)^2$ versus the photon energy gives the direct band gap of 1.4 and 1.53 eV for synthesized and annealed powder samples. These values match well with the literature values [21, 32, 35] and indicate that material is efficient for solar energy conversion. It is observe that band gap of the sample increases on annealing, it may be due to the ordering within nanocrystals and increase in crystalline nature.

3.5 Photocatalytic degradation of MB dye

Annealed CZTS powder was used as a catalyst for the photocatalytic dye degradation. Methylene blue has been taken

as a model dye whose degradation was studied at the characteristic wavelength at 664 nm with the help of UV–Vis spectrometer. Figure 5 shows characteristic peak of MB blank solution and effect of addition of 25 mg of CZTS as a catalyst. The absorption spectra MB without catalyst shows maximum intensity at $\lambda_{max} = 664$ nm and over a period 6-h no degradation observed under a dark and light condition showing that MB itself is stable and cannot be degraded on its own. On addition of catalyst and exposure to visible light, 50% reduction in characteristic peak within 45 min. was observed, which is calculated by using Eq. (1).

Figure 6a demonstrates the degradation rate of MB without catalyst and with CZTS as a catalyst under the visible radiation. Without catalyst no significant degradation was observed whereas with catalyst degradation efficiency of MB clearly increased. First order rate constant has been calculated from Eq. (2), is shown by Fig. 6b. The apparent first order reaction rate constant (k_{app}) was found to be 0.018 min^{-1}. To gain the insight of activity, the equation:

$k = \frac{k_{app}}{m}$ gives the activity parameter of catalyst, where m is the mass of loaded catalyst [36]. It was found to be 0.72 min^{-1} g^{-1}.

Possible mechanism of degradation of MB dye in presence of CZTS which acts as a catalyst on exposure to the light is described in Eqs. (7–12) and schematically shown in Scheme 1 [36],
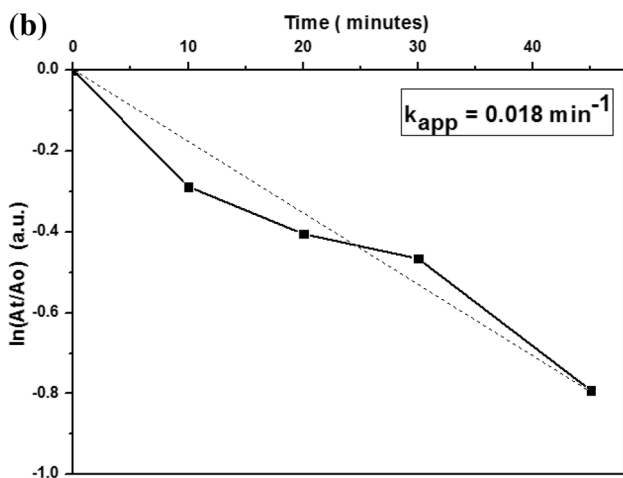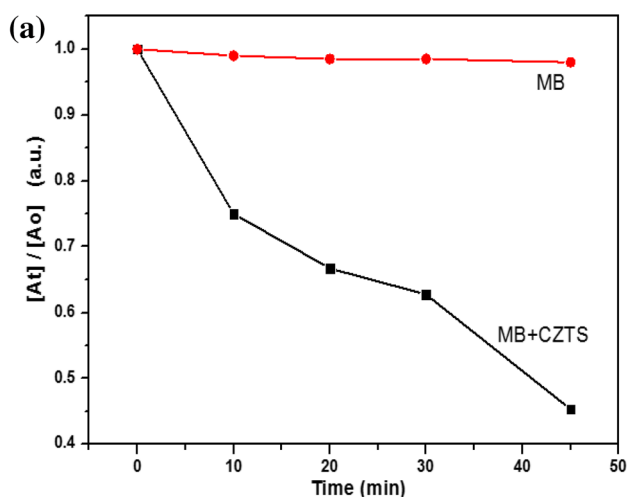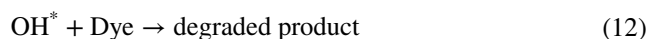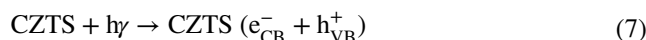
$$CZTS + h\gamma \rightarrow CZTS\ (e^-_{CB} + h^+_{VB}) \tag{7}$$

$$H_2O + h^+_{VB} \rightarrow OH^* + H^+ \tag{8}$$

$$O_2 + e^-_{CB} \rightarrow O_2^{-*} \tag{9}$$

$$O_2^{-*} + H_2O \rightarrow H_2O_2 \tag{10}$$

$$H_2O_2 \rightarrow 2OH^* \tag{11}$$

$$OH^* + Dye \rightarrow degraded\ product \tag{12}$$

4 Conclusion

CZTS nanoparticle of crystallite size 29 nm was synthesized via a simple and green hydrothermal method. Kesterite phase of CZTS was confirmed by XRD and Raman analysis. SEM analysis reveals the agglomeration of nanoparticles. UV–Vis spectroscopic study gives optical band gap of 1.53 eV suggesting CZTS as a good visible light absorber material. The CZTS powder has been used as a catalyst for the degradation of methylene blue in aqueous solution. Photocatalysis results reveal that 50% degradation of MB was achieved when exposed to 45 min. of irradiation at the rate of reaction 0.018 min^{-1}. The further research is
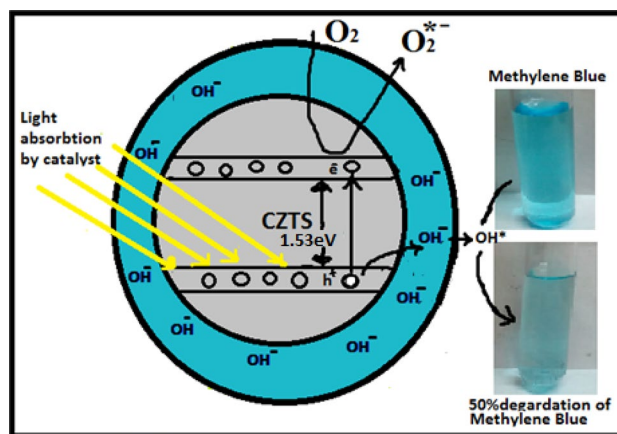

Fig. 6 a Plot of $[A_t]/[A_o]$ against reaction time t, b plot of $\ln(A_t/A_o)$ against time t for evaluating rate constant k_{app} for MB

Scheme 1 Schematic representation of degradation of MB by using CZTS as a catalyst on exposure to light

based on analyzing the details of degradation of MB dye with the help of CZTS as a catalyst.

References

1. V.S. Shrivastava, Photocatalytic degradation of Methylene blue dye and Chromium metal from wastewater using nano crystalline TiO_2 Semiconductor. Arch. Appl. Sci. Res. **4**, 1244 (2012)
2. X. Hou, Highly efficient photocatalysis of p-type Cu_2ZnSnS_4 under visible-light illumination. Mater. Res. Bull. **60**, 628 (2014)
3. H. Lu, Hierarchical ZnO micro architectures assembled by ultrathin nano sheets: hydrothermal synthesis and enhanced photocatalytic activity. J. Mater. Chem. **21**, 4228 (2011)
4. S.B. Kokane, Photocatalytic performance of Pd decorated TiO_2-CdO composite: role of in situ formed CdS in the photocatalytic activity. Int. J. Hydrog. Energy **40**, 13431 (2015)
5. O. Sacco, Photocatalytic degradation of organic dyes under visible light on n-doped TiO_2 photocatalysts. Int. J. Photoenergy **2012**, 626759 (2012)
6. K.V. Gurav, Electrosynthesis of CZTS films by sulfurization of CZT precursor: effect of soft annealing treatment. Appl. Surf. Sci. **283**, 74 (2013)
7. U. Ghorpade, Towards environmentally benign approaches for the synthesis of CZTSSe nanocrystals by a hot injection method: a status review. Chem. Commun. **50**, 11258 (2014)
8. P. Kush, Efficient hydrogen/oxygen evolution and photocatalytic dye degradation and reduction of aqueous Cr(VI) by surfactant free hydrophilic Cu_2ZnSnS_4 nanoparticles. J. Mater. Chem. **A3**, 8098 (2015)
9. X. Yu, Cu_2ZnSnS_4-Pt and Cu_2ZnSnS_4-Au heterostructured nanoparticles for photocatalytic water splitting and pollutant degradation. J. Am. Chem. Soc. **136**, 9236 (2014)
10. J. Wang, Surfactant- free hydrothermal synthesis of Cu_2ZnSnS_4 (CZTS) nanocrystals and photocatalytic properties. RSC Adv. **4**, 27805 (2014)
11. L. Rovelli, Optimization and stabilization of electrodeposited Cu_2ZnSnS_4 photocathodes for solar water reduction. ACS Appl. Mater. Interfaces **5**, 8018 (2013)
12. K. Ito, Characterization of Cu_2ZnSnS_4 thin films prepared by vapor phase sulfurization, Jpn. J. Appl. Phys. **27**, 2094 (1988)
13. V.A. Madiraju, CZTS synthesis in aqueous media by microwave irradiation. J. Mater. Sci. **27**, 3152 (2016)
14. G.L. Agawane, Synthesis of simple, low cost and benign sol–gel Cu_2ZnSnS_4 thin films: influence of different annealing atmospheres. J. Mater. Sci. **26**, 1900 (2015)
15. S.S. Mali, Polyvinylpyrrolidone (PVP) assisted single-step synthesis of kesterite Cu_2ZnSnS_4 nanoparticles by solvothermal process. Phys. Status Solidi RRL **12**, 1050 (2013)
16. M. Suryawanshi, The synergistic influence of anionic bath immersion time on the photo electrochemical performance of CZTS thin films prepared by a modified SILAR sequence. RSC Adv. **4**, 18537 (2014)
17. D. Xia, Synthesis and characterization of Cu_2ZnSnS_4 nano crystals by hot-injection method. J. Mater. Sci. **26**, 5426 (2015)
18. E.M. Mkawi, Influence of substrate temperature on the properties of electrodeposited kesterite Cu_2ZnSnS_4 (CZTS) thin films for photovoltaic applications. J. Mater. Sci. **26**, 222 (2015)
19. B. T. Jheng, Promising sputtering route for dense Cu_2ZnSnS_4 absorber films and their photovoltaic performance. Sol. Energy Mater. Sol. Cells 128 (2014) 275.
20. S. A. Vanalakar, Effect of post annealing atmosphere on the grain-size and surface morphological properties of pulsed laser deposited CZTS thin films, Ceram. Int. **40**, 15097 (2014)
21. W.C. Liu, Facile hydrothermal synthesis of hydrotropic Cu_2ZnSnS_4 nanocrystal quantum dots: band-gap engineering and phonon confinement effect. J. Mater. Chem. A **1**, 3182 (2013)
22. S.S. Mali, Novel synthesis of kesterite Cu_2ZnSnS_4 nanoflakes by successive ionic layer adsorption and reaction technique: characterization and application. Electrochim. Acta **66**, 216 (2012)
23. K.V. Gurav, Cu_2ZnSnS_4 (CZTS)-based room temperature liquefied petroleum gas (LPG) sensor. Sens. Actuators B **190**, 408 (2014)
24. M. Lashgari, A nanocomposite p-type semiconductor film for possible application in solar cells: photo-electrochemical studies. Sol. Energy Mater. Sol. Cells 137 (2015) 274.
25. D.Y. Yun, Memory stabilities and mechanisms of organic bistable devices with giant memory margins based on Cu_2ZnSnS_4 nanoparticles/PMMA nanocomposites. Org. Electron. **24**, 320 (2015)
26. S. Chakrabarti, Multilevel memristor effect in metal–semiconductor core–shell nanoparticles tested by scanning tunneling spectroscopy. Nanoscale **7**, 9886 (2015)
27. K. Zhang, Composition control in Cu_2ZnSnS_4 thin films by a sol–gel technique without sulfurization. J. Mater. Sci. **25**, 2703 (2014)
28. M. Suryawanshi, Kesterite CZTS nanocrystals: pH-dependent synthesis. Physica Status Solidi A **211**, 1531 (2014)
29. S.A. Vanalakar, Controllable synthesis of stiochiometric Cu_2ZnSnS_4 nanoparticles by solvothermal method and its properties. API Conf. Preceding **1665**, 050061 (2015)
30. P. Kush, Development and properties of surfactant-free water dispersible Cu_2ZnSnS_4 nanocrystals: a material for low cost photovoltaics. ChemPhysChem **14**, 2793 (2013)
31. S.S. Mali, Low-cost electrospun highly crystalline kesterite Cu_2ZnSnS_4 nanofiber counter electrodes for efficient dye-sensitized solar cells. ACS Appl. Mater. Interfaces **6**, 1688 (2014)
32. G. Rajesh, Solution-based synthesis of high yield CZTS (Cu_2ZnSnS_4) spherical quantum dots. Superlattices Microstruct. **77**, 305 (2015)
33. S. Sarkar, Self-sacrificial template directed hydrothermal route to kesterite-Cu_2ZnSnS_4 microspheres and study of their photo response properties. CrystEngComm **16**, 2634 (2014)
34. Z. Zou, One-pot solvothermal synthesis of wurtzite Cu_2ZnSnS_4 nanocrystals, Mater. Lett. **158**, 13 (2015)
35. Y. Zhao, Synthesis and characterization of Cu_2ZnSnS_4 nanocrystals prepared by microwave irradiation method. J. Mater. Sci. **26**, 5645 (2015)
36. P. Kush, Anisotropic kesterite $Cu_2ZnSnSe_4$ colloidal nanoparticles: photoelectrical and photocatalytic properties. Mater. Chem. Phys. **162**, 608 (2015)